Journal of Zhejiang University-SCIENCE A 2026 27(3):262-274
www.jzus.zju.edu.cn; www.springer.com/journal/11582
E-mail: jzus_a@zju.edu.cn

Research Article
https://doi.org/10.1631/jzus.A2500160

Check for updates

Economic analysis and impact assessment of electricity supply and demand-side emission reductions in China under carbon neutrality goals

Xuanxuan MING[1], Qiang WANG[1,2]✉, Kun LUO[1,2]✉, Xinhao DU[1], Jianren FAN[1,2]

[1]*State Key Laboratory of Clean Energy Utilization, Department of Energy Engineering, Zhejiang University, Hangzhou 310027, China*
[2]*Zhejiang Key Laboratory of Clean Energy and Carbon Neutrality, Hangzhou 310027, China*

Abstract: The power sector is one of the largest carbon emitters in China and faces nonlinear cost impacts from different emission reduction measures across regions with varying electricity demand characteristics. In this study, we analyze the effects and cost efficiency of supply-side and demand-side emission reduction pathways by classifying Chinese provinces into four categories. This is accomplished through integration of the Next Energy Modeling System for Optimization (NEMO) and the Low Emissions Analysis Platform (LEAP), i.e., LEAP-NEMO. Applying this method, our results show that urbanization will likely drive stable growth in residential electricity demand, while industrial development will vary regionally. Resource-rich regions require wind and solar energy as foundational methods to decarbonize their mix of electricity sources, whereas areas with limited natural resources need nuclear energy and alternative energy generation technologies to mitigate supply gaps. Furthermore, we find that delaying the emission peak year raises marginal carbon reduction costs and the cumulative cost per unit of carbon abatement. A 1.5% reduction in energy intensity is the most cost-effective for the majority of regions.

Key words: Power systems; Low Emissions Analysis Platform-Next Energy Modeling System for Optimization (LEAP-NEMO); Clean energy transition; Energy consumption

1 Introduction

Greenhouse gas emissions have contributed to global warming, resulting in a global surface temperature increase of 1.1 °C above pre-industrial levels during the period of 2011–2020 (IPCC, 2023). Human-induced climate change has caused widespread adverse effects on food and water security, human health, economic systems, and societal structures, resulting in significant losses and damage to both natural ecosystems and human communities. As one of the largest contributors to CO_2 emissions, China has pledged to stop increasing its carbon emissions by 2030 and achieve carbon neutrality by 2060 (Li et al., 2022). The electricity sector is a major contributor to carbon emissions in China, being responsible for over 50% of the country's total coal consumption (Fan et al., 2023). Specifically, coal-fired power generation alone comprises approximately 43% of China's total CO_2 emissions (Yu et al., 2021). This highlights the need for sustainable alternatives in the electricity generation sector to mitigate environmental impacts. The objective of the "14th Five-Year Plan for a Modern Energy System" is to establish a new type of power system by optimizing the electrical grid through the integration of supply- and demand-side measures. Reforms on the supply side promote the development of renewable energy industries (Elsisi and Abdelfattah, 2020; Yap et al., 2020; Wang et al., 2023), while demand-side management aims to minimize energy dissipation (Besagni et al., 2020). Both strategies are fundamental for achieving carbon neutrality in the power sector. However, determining the optimal integration of these control measures to reduce CO_2 emissions in the power system remains a significant challenge.

✉ Qiang WANG, zjuqw@zju.edu.cn
Kun LUO, zjulk@zju.edu.cn
Xuanxuan MING, https://orcid.org/0009-0008-5788-2733
Qiang WANG, https://orcid.org/0000-0002-9782-6575
Kun LUO, https://orcid.org/0000-0003-3644-9400

Received Apr. 30, 2025; Revision accepted July 31, 2025;
Crosschecked Dec. 18, 2025; Online first Feb. 14, 2026

Prevailing supply-side research methodologies are increasingly adopting more sophisticated and flexible approaches. This evolution has broadened the analytical scope, shifting from a sole focus on electrical power equilibrium to consideration of carbon emission constraints. The main objective of most studies has been to achieve optimal flexibility while minimizing costs within these limitations (Cai et al., 2022; Handayani et al., 2022, 2023). For instance, Awopone et al. (2017) utilized the Open Source Energy Modelling System in conjunction with the Low Emissions Analysis Platform (LEAP) to examine the least-cost development of a system under a no-policy-change scenario, specifically exploring optimal energy generation strategies for Ghana from 2010 to 2040. Furthermore, Ma et al. (2021) proposed a novel model and optimal dispatch for combined heat and power with a power-to-gas (P2G) and carbon capture system. In addition, Wang et al. (2020) adopted a multiscale framework to optimize wind farm layouts without altering electricity demand. However, the above studies have not accounted for the constraints of renewable energy resources in different regions. Meanwhile, the Next Energy Modeling System for Optimization (NEMO) stands out as capable of representing such multiple objective constraints.

The primary approach of demand-side research has been to forecast electricity consumption through the synergistic optimization of various low-carbon power technologies and emission reduction strategies (Schäfer et al., 2016; Ming et al., 2024). For example, Zhou JH et al. (2023) proposed a novel hierarchy for electricity demand influencers based on a CO_2 emission intensity constraint within the industrial sector and forecasted electricity demand under various policy constraint scenarios. Moreover, Rao et al. (2024) adopted an optimal economic framework for electricity demand forecasting, calibrating historical GDP statistics with a nighttime light dataset. Later, they developed an error correction model based on electricity data to predict electricity consumption trends in the Pearl River Delta region in China under different carbon emission scenarios. In another study, Wu et al. (2021) analyzed the energy demand and carbon emissions in the Yangtze River Delta region in China from 2020 to 2050 under different energy transition scenarios.

Recent studies have explored the synergistic coupling effects between supply and demand in power systems (Zhou et al., 2023). The literature has extensively focused on energy supply and demand optimization for individual regions or countries, utilizing a variety of methods. For instance, Liu et al. (2022) comprehensively accounted for the spatiotemporal variations in wind and solar power generation in China, instantaneous electricity demand across various societal sectors, land use, government policies, and renewable energy development strategies. They applied a mixed-integer linear programming (MILP) model to optimize the configuration of wind and solar systems within each grid, including the location and installed capacity of wind and photovoltaic power plants, and evaluated the economic costs and environmental benefits of different solutions. In addition, Jia et al. (2022) established a dynamic multiobjective optimization model, optimizing the power generation structure to align with future development scenarios in China. This approach explored the optimal pathways for carbon emissions, economic growth, and energy consumption within the context of differing scenarios. Moreover, Yang et al. (2023) constructed a novel integrated two-stage emission reduction model, emphasizing joint emission reduction from both the demand and supply sides. However, the studies above were primarily based on localized optimization or short-time-scale models and did not systematically analyze the variability and feasibility of coordinated strategies across regions with varying electricity supply and demand characteristics. In contrast to previous studies, we adopt the integrated Low Emissions Analysis Platform-Next Energy Modeling System for Optimization (LEAP-NEMO) framework, which enables systematic modeling of energy system dynamics across extended temporal scales. In terms of policy evaluation, we explore the independent optimization of demand-side and supply-side measures and further analyze their synergistic effects in different scenarios. In this way, the similarities and differences between different types of regions in achieving the lowest cost emission reduction pathways are revealed.

To this end, we categorize 31 provincial-level administrative regions in China into four representative regions based on their electricity supply and demand profiles, enabling a regionally variable analysis. We assess the effectiveness and economic feasibility of various emission reduction strategies on both the supply and demand sides within these regions, providing

insights that may aid policy promoting China's carbon neutrality goals. The novelty of this study lies in three main aspects: (i) developing a regional classification framework based on electricity supply and demand features to analyze the impact of heterogeneity on emission pathways; (ii) proposing integrated supply-demand optimization methods for cost-effective emission reductions; (iii) assessing the impact of different peak carbon emission timelines on the cost of achieving net-zero carbon emissions.

2 Region classification and methodology

2.1 Region classification

Based on median values of electricity generation and demand data, we classified 31 provincial-level administrative regions (excluding Hongkong, Macao, and Taiwan) in China into four distinct categories, as illustrated in Fig. 1. Note that LH stands for the low generation and high demand region, HH stands for the high generation and high demand region, LL stands for the low generation and low demand region, and HL stands for the high generation and low demand region. Shandong stands out as the province with the highest electricity supply and demand in China, while Xizang is the region with the lowest. Detailed electricity generation and demand data for each province are given in Table S1 of the electronic supplementary materials (ESM).

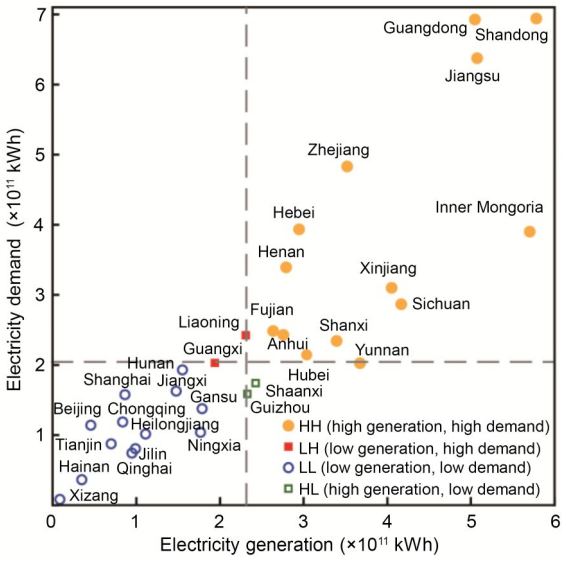

Fig. 1 Classification of regions according to electricity generation and demand

From the perspective of the regional economy and electricity demand, high demand regions (HH and LH) are predominantly concentrated in the economically developed eastern coastal provinces (e.g., Guangdong, Jiangsu, and Zhejiang) and certain inland core provinces (e.g., Sichuan). These areas are characterized by dense industrial clusters, high population density, and strong economic activity, leading to substantial electricity consumption. In contrast, low-demand regions (HL and LL) are primarily distributed in the relatively underdeveloped northwestern and northeastern regions, where economic output and population density are comparatively lower. Regarding resource endowment and power generation capacity, high generation regions (HH and HL), such as Inner Mongolia and Shanxi, leverage abundant coal resources and large-scale thermal power installations to achieve high electricity output. Meanwhile, southwestern provinces such as Yunnan and Sichuan have capitalized on their rich hydropower resources to become hubs for clean energy generation. Conversely, some core cities (e.g., Beijing and Shanghai), which are constrained by limited natural resources and/or stringent environmental policies, exhibit lower local power generation capacity and thus heavily depend on external electricity transmission to meet demand.

2.2 Model framework

This study employs LEAP-NEMO, which integrates the energy system optimization tool NEMO into the original LEAP. The calculation of LEAP encompasses end-use demand analysis, energy transformation calculations, transmission loss analysis, environmental emission impact estimations, and cost–benefit analysis (Rogan et al., 2014). The modeling framework and key inputs of LEAP-NEMO used in this study are illustrated in Fig. 2. The LEAP model serves as the foundation of this research and is primarily focused on describing three core parameters of the energy system: electricity generation, energy transformation, and end-use energy demand. The end-use energy demand encompasses multiple industries and sectors, including agriculture, industry, construction, TSAP (transportation, storage, and postal), WRTHC (wholesale and retail, trade, hotel, and catering services), and residential services. On the other hand, electricity generation focuses on aspects such as energy load shape, process efficiency, capacity credit, maximum availability, and equipment lifetime. Based on these

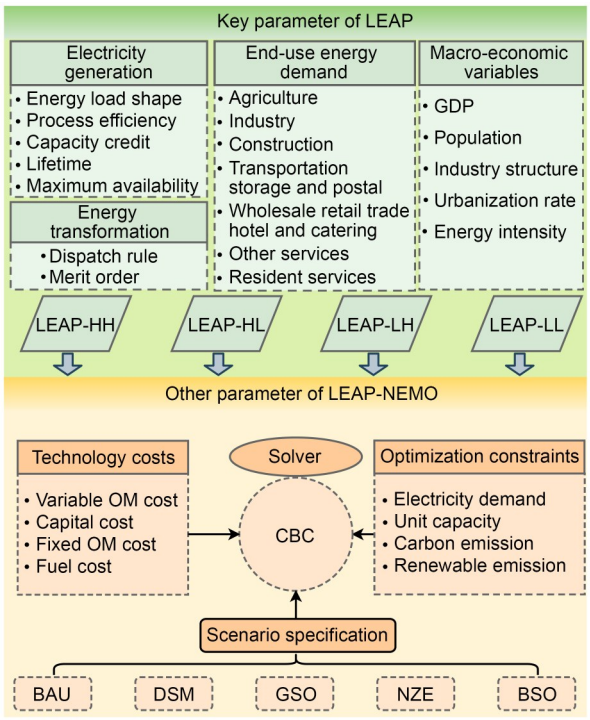

Fig. 2 Modeling framework and key inputs of LEAP-NEMO. BAU: business as usual; DSM: demand-side management; GSO: generation sector optimization; NZE: net-zero emission; BSO: both sides optimization

parameters, we use LEAP to construct energy models for the four different types of regions.

The NEMO module is integrated into the LEAP model to enable advanced optimization analysis of the energy system. LEAP-NEMO aims to minimize the total social cost of the system. The required inputs for technical costs include Variable OM (operation and maintenance) Cost, Capital Cost, Fixed OM Cost, and Fuel Cost. The optimization process is constrained by several factors, including electricity demand, unit capacity, carbon emissions, and renewable energy emissions. The model defines multiple future scenarios to evaluate carbon emission pathways and their associated mitigation costs under various supply- and demand-side emission reduction strategies. To determine the planning and optimization of the power generation structure, NEMO integrates multiple solvers, such as Coin-or Branch and Cut (CBC), IBM ILOG CPLEX Optimizer (CPLEX), and Dual Linear Programming Kit (DLPK), which provide efficient computational support for the optimization of the energy system.

2.3 Calculation principles

2.3.1 Population projection

A survival transition matrix was constructed based on the actual population status of the statistical region (Wang, 2018).

$$nP_{t_2}(x+n)=nP_{t_1}(x)\times\frac{nL(x+n)}{nL(x)}, \tag{1}$$

where n represents both the age group interval and the projection interval in years between the initial time point (t_1) and the projected time point (t_2). x denotes the starting age of an age group at t_1 and it ranges from 0 to 100 years old. $nP_{t_1}(x)$ represents the number of people aged [x, x+n] at time t_1, and $nP_{t_2}(x+n)$ is the number of people aged [x+n, x+2n] at time t_2. $nL(x)$ is the number of person-years lived by those exactly aged [x, x+n] in the cohort, and $nL(x+n)$ represents the number of person-years lived by those exactly aged [x+n, x+2n] in the cohort. Here, person-years is a measure that accounts for both the number of people and the amount of time each person contributes to the cohort. For example, 100 people each living 1 year equals 100 person-years.

The fertility model is established based on the survival transition matrix:

$$P_{t_2}(0)=\sum\left[nP_{f_{t_1}}(x)\cdot nF(x)+nP_{f_{t_1}}(x)\cdot nF(x+n)\cdot\frac{nL(x+n)}{nL(x)}\right]\cdot\frac{L(0)}{2}, \tag{2}$$

where $P_{t_2}(0)$ represents the number of people aged 0 at time t_2, and $nP_{f_{t_1}}(x)$ is the number of women aged [x, x+n] at time t_1, with x ranging from [15, 49]. $nF(x)$ and $nF(x+n)$ represent the fertility rates of women of childbearing age in the age ranges of [x, x+n] and [x+n, x+2n], respectively.

The total population at t_2 is:

$$T_{t_2}=\sum nP_{t_2}(x), \tag{3}$$

where $nP_{t_2}(x)$ represents the number of individuals aged [x, x+n] at time t_2.

2.3.2 Cost of electricity generation

The method for calculating the total cost M of electricity generation is presented as follows (Cai, et al., 2022):

$$M=\sum_{i}^{n}(f_jC_j+o_jC_j+V_jP_j+E_j), \tag{4}$$

where f_j denotes the capital cost of power technology j, o_j is the fixed cost of operations and maintenance, C_j is the installed capacity, V_j is the variable cost, P_j represents the power generation, and E_j represents the fuel cost.

2.3.3 Marginal cost for carbon emission reduction

The marginal cost of carbon reduction C_{MA} is defined as the ratio of the additional cost ΔC to the amount of carbon reduction ΔR incurred from implementing emission reduction technologies relative to a baseline scenario (Schäfer et al., 2016). The specific formula for this quantity is:

$$C_{\mathrm{MA}}=\frac{\Delta C}{\Delta R}. \tag{5}$$

The marginal cost growth rate for carbon reduction R refers to the rate of increase in the marginal cost of carbon reduction by a specified year. Its expression is:

$$R=\left(\frac{V_{\mathrm{e}}}{V_{\mathrm{s}}}\right)^{\frac{1}{N}}-1, \tag{6}$$

where V_{e} and V_{s} represent the marginal cost of carbon reduction at the specified end year and start year, respectively, and N denotes the difference in years.

The total cost per unit of carbon reduction C_{ucr} refers to the cumulative marginal cost of carbon reduction over a given period of time t. Its specific formula is:

$$C_{\mathrm{ucr}}=\int_t C_{\mathrm{MA}}(t)\cdot \mathrm{d}t. \tag{7}$$

2.3.4 Model optimization constraints

To solve the MILP problems in the model, we selected the CBC solver. CBC employs a Branch-and-Bound algorithm as its core framework (Lee and Mitchell, 2009). As such, it systematically explores all possible solution candidates but uses branching to subdivide the problem domain, progressively narrowing the search range and using upper and lower bounds to exclude areas that cannot contain the optimal solution. We utilize the heuristic best bound branching strategy, along with activating the strong cutting plane strategy during the solution process in the CBC solver. These algorithmic choices are designed to improve computational efficiency and effectively address the complexities of the optimization problem. The optimization objective function is as follows:

$$D=\sum_i A_i\times I_i, \tag{8}$$

where D is the sum of the electricity demands of various industries, A_i represents the activity levels of electricity consumption in various sectors, and I_i represents the energy intensity of the corresponding activity.

The first type of constraint is the electricity demand, which is that the power transformation G (i.e., the power supply) needs to meet the terminal electricity demand D:

$$G=\sum_j g_j=\sum_j C_j\times\alpha_j\times\beta_j\geqslant D+\sum_j L_j, \tag{9}$$

$$L_j=g_j\times l_j, \tag{10}$$

$$\alpha_j\times\beta_j\leqslant U_j, \tag{11}$$

where g_j represents the actual power supplies of different types, α_j denotes capacity credit, β_j refers to the maximum availability, L_j indicates the transmission losses for various types of power generation, l_j is the corresponding transmission loss rate, and U_j refers to the upper limit of the operating rate.

The second type is the unit capacity constraint, which means that the total installed capacity of the region should meet the annual maximum load demand of the power system to ensure safe and stable operation of the system.

$$\sum_j C_j\times(1+r)\geqslant d, \tag{12}$$

where r refers to the reserve margin, and d is the annual maximum load demand.

The third type is an emission constraint, wherein the CO_2 emissions of the power system need to reach

net-zero by 2060 while also meeting the desired carbon emission peak.

$$\begin{cases} G_{2060} = 0, & (13) \\ G_{2030} \geqslant G_y, \ y \in [2020, 2060]. & (14) \end{cases}$$

The fourth type is the renewable energy constraint. The renewable resources consumed by the generating units cannot exceed the upper limit of the local region's resource potential $e_{\max}$. Its expression is as follows:

$$e_j \leqslant e_{j,\max}. \quad (15)$$

2.3.5 Energy intensity sensitivity analysis

Sensitivity analysis is used to study how uncertainty in a model's outputs is apportioned to different sources of uncertainty in its inputs (Saltelli, 2002). In dealing with problems involving multiple input variables, sensitivity analysis helps reveal the strengths and correlations between inputs and outputs (Saltelli et al., 2007). We use the elasticity of cost increase concerning the rate of reduction in energy intensity as a measure of the sensitivity S. The formula is as follows:

$$S = \frac{\Delta C}{\Delta I}, \quad (16)$$

where ΔI represents the rate of energy intensity reduction adopted in other scenarios relative to the baseline scenario.

2.4 Scenario setting and description

In addition to the business as usual (BAU) scenario, we introduce four distinct scenarios categorized into two main categories: single-factor control on either the supply or demand side and coupled control. On the demand side, single-factor control is exemplified by the demand-side management (DSM) scenario. For the supply side, single-factor control is represented by two scenarios: the generation sector optimization (GSO) scenario and the net-zero emission (NZE) scenario. The scenario involving coupled control of supply and demand is primarily the both sides optimization (BSO) scenario.

2.4.1 Business as usual scenario

The data used for electricity demand modeling primarily originate from the 2020 Statistical Yearbook of the 31 provinces and cities in China (National Bureau of Statistics of China, 2020) and the Seventh National Population Census (National Bureau of Statistics of China, 2021). In the industrial sector, GDP is used to represent the activity level, while electricity consumption per GDP indicates the energy intensity. In the residential sector, population is used to represent the energy activity level, and per capita electricity consumption is used for energy intensity. Based on the industrial activity levels and elasticity coefficients of various provinces from 2010 to 2020, the development of the industrial sector can be reasonably extrapolated.

In terms of electricity supply modeling, the construction of installed capacity is based on regional electricity generation data from the 2020 China Electric Power Yearbook (China Electricity Council, 2021). The costs of different power generation technologies are detailed in Table S2, primarily referencing Wang XG et al. (2023) and Zhou WD et al. (2023). The electricity load curves of four regions are shown in Fig. S1 of the ESM. The parameters for the elasticity coefficients of the industrial activity levels in the four regions are provided in Table 1.

Table 1 Elasticity coefficient parameters of industry activity levels

Industry	Elasticity coefficient			
	LH	HH	LL	HL
Agriculture	1.82%	2.50%	2.47%	2.25%
Industry	2.21%	2.84%	1.91%	1.73%
Construction	2.31%	5.36%	3.17%	4.98%
TSAP	1.40%	4.60%	2.24%	2.20%
WRTHC	2.77%	5.25%	4.90%	3.57%
Other services	1.24%	8.69%	6.51%	5.34%

Higher elasticity coefficients indicate a sector's increased sensitivity to energy activity levels. In the four regions, the construction sector and the WRTHC sector generally exhibit higher elasticity coefficients. Apart from the LH region, the elasticity coefficients for other industries in the regions consistently exceed 5%.

2.4.2 Demand side management scenario

The DSM scenario mainly focuses on adjusting the energy intensity of various industries and

livelihood-related areas in the four regions. Historical data show that the global average annual reduction rate of energy intensity is approximately 1.2% (Goldemberg and Prado, 2013). Ming et al. (2024) set a 2% reduction for high energy consumption industries and a 0.5% reduction rate for low energy consumption industries in Zhejiang Province. Based on these references, we adopt a 1.5% energy intensity reduction rate. Note that the parameter settings for the electricity transformation are consistent with those of the BAU scenario. Table 2 shows the initial energy intensity settings for different industries in the four regions.

Table 2 Initial energy intensity parameters in the four regions

Industry	Initial energy intensity ($\times10^{-3}$ kWh/CNY)			
	LH	HH	LL	HL
Agriculture	10.76	29.65	14.37	9.96
Industry	227.51	163.08	140.06	154.48
Construction	7.88	13.85	13.12	14.90
TSAP	24.41	41.64	58.46	63.54
WRTHC	39.20	27.34	38.65	59.91
Other services	31.50	21.52	16.54	15.44

2.4.3 Generation sector optimization and net-zero emission scenario

When exploring the impact of supply-side emission reduction, two scenarios are considered: the GSO scenario and the NZE scenario. The GSO scenario utilizes LEAP-NEMO to optimize the power generation mix toward a minimum cost objective, considering actual resource constraints without carbon emission constraints while maintaining constant energy intensity on the demand side. The distinction between the NZE and the GSO is the additional carbon emission constraint in the NZE scenario. Specifically, the NZE scenario stipulates that the power sector should reach its peak CO_2 emissions in 2030, 2040, and 2050 and achieve net-zero CO_2 emissions by 2060. The power generation structures of the four regions in 2020 are analyzed in Table 3.

2.4.4 Both sides optimization scenario

The BSO scenario, which encompasses modifications on both the demand and supply sides, tests the optimal rate of energy intensity reduction (set at 1.0%, 1.5%, and 2.0%) for different regions. Moreover, it incorporates optimization of the minimum cost on the generation side under carbon emission constraints. A summary of parameter adjustments across the different scenarios is presented in Table 4.

Table 3 Power generation structures of the four regions in 2020

Power generation	Proportion (%)			
	LH	HH	LL	HL
Coal	75.57%	73.47%	77.79%	76.05%
Wind	5.74%	4.08%	5.66%	2.24%
Solar	1.79%	4.08%	5.32%	6.27%
Nuclear	4.78%	8.16%	0.81%	–
Hydro	12.09%	10.20%	5.32%	15.40%

Table 4 Comparison of parameter settings for four special scenarios in the BAU scenario

Scenario	Energy intensity reduction rate	Minimum cost optimization	Carbon emission constraint
DSM	1.5%	Off	–
GSO	0.0%	On	–
NZE	1.5%	On	Net-zero in 2060
BSO	1.0%–2.0%	On	Net-zero in 2060

3 Results and discussion

3.1 Proportion of electricity consumption in demand-side industries

We begin with a demand-side analysis of the BAU scenario, as shown in Fig. 3. The inner part of the ring highlights industries experiencing a reduction in electricity consumption share, while the outer portion indicates those with an increased proportion. The continued growth in the electricity consumption share of the agricultural sectors within both the HH and LL regions indicates persistent potential for modernization in these areas. For the HH region, the rising share of agricultural sectors likely stems from expanding electrification demand in urban agriculture. Priority should be given to optimizing time-of-use electricity price adaptability for facility-based agricultural systems. On the other hand, a systematic assessment of the levelized cost of electricity for photovoltaic-integrated irrigation systems is recommended for the LL region. The marginal variations observed in electricity consumption within the LH and HL regions suggest an approaching saturation point in the developmental trajectory of this sector. The industrial sector in the LH

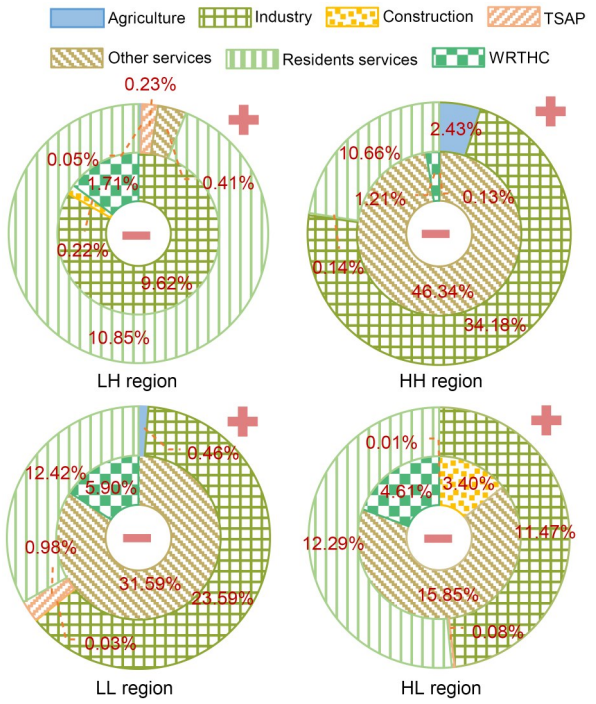

Fig. 3 Changes in electricity consumption share by demand-side industries from 2020 to 2060 in the four regions (the inner ring indicates a decrease, and the outer ring indicates an increase)

region is expected to decline, which may require intervention such as establishing a coordinated industrial relocation compensation fund to prevent deindustrialization. In contrast, industrialization in the remaining three regions is expected to progress. In terms of residential electricity consumption, a consistent rise across all regions underscores China's ongoing urbanization efforts. The construction sector in the HL region experiences a significant decline in electricity consumption share, while it remains relatively stable in other regions, indicating that no significant structural changes occur. The share of the TSAP sector marginally increased in the LH and LL regions, which stands in contrast to a universal decline in the WRTHC sector across all regions, reflecting a downturn in this sector within China. Other services in the LH region see a minor uptick in electricity consumption share, yet they still follow the overall national downward trend.

3.2 Changes in power generation structure

Fig. 4 displays the decadal changes in the power generation structure from 2020 to 2060. From the perspective of the dominant regional power generation methods, wind energy exhibits the highest rate of expansion in the LH region, whereas solar photovoltaic generation spearheads growth in the other regions. Analyzing the changes in the proportion of various power generation methods, wind power shows its largest proportional increase in the LH region (37.70%) and its smallest in the HL region (21.26%). Solar power experiences the highest proportional growth in the HH region (32.28%) and its lowest in the LH region (22.93%). Nuclear energy's share increases the most in the HL region (8.05%), while LL sees a minimal increase (0.77%). Hydropower's share expands most significantly in the HL region (22.94%), whereas the HH region records the smallest increase (8.08%). Furthermore, studies have revealed that low-generation regions generally suffer from scarce wind and solar energy resources. Thus, to meet future electricity demands, these areas may require targeted development of nuclear and hydropower infrastructure. However, it should be noted that the central and southern regions exhibit limited potential for new hydropower development. Consequently, future development strategies in these areas should focus on capacity expansion and efficiency improvements at existing hydropower stations rather than pursuing new construction projects. Moreover, the large-scale deployment of renewable energy in China faces challenges such as intermittency-related grid integration issues, insufficient long-distance transmission capacity, land-use and ecological constraints, and financing barriers. To overcome these issues, policy measures such as grid modernization, electricity market reforms, financial incentives, and coordinated land-energy planning are essential for supporting a balanced and low-carbon power system.

3.3 Marginal cost of carbon emission reduction in different peak years

The primary difference between GSO and NZE is that the GSO scenario excludes carbon emission restrictions, while the NZE scenario explicitly accounts for them. Consequently, the cost difference between these scenarios relative to the total carbon reduction achieved serves as an indicator of the marginal cost of carbon mitigation. The NZE scenario establishes three subscenarios for different peak years in the power sector, facilitating an exploration of the impact of different peak years on the marginal cost of carbon reduction.

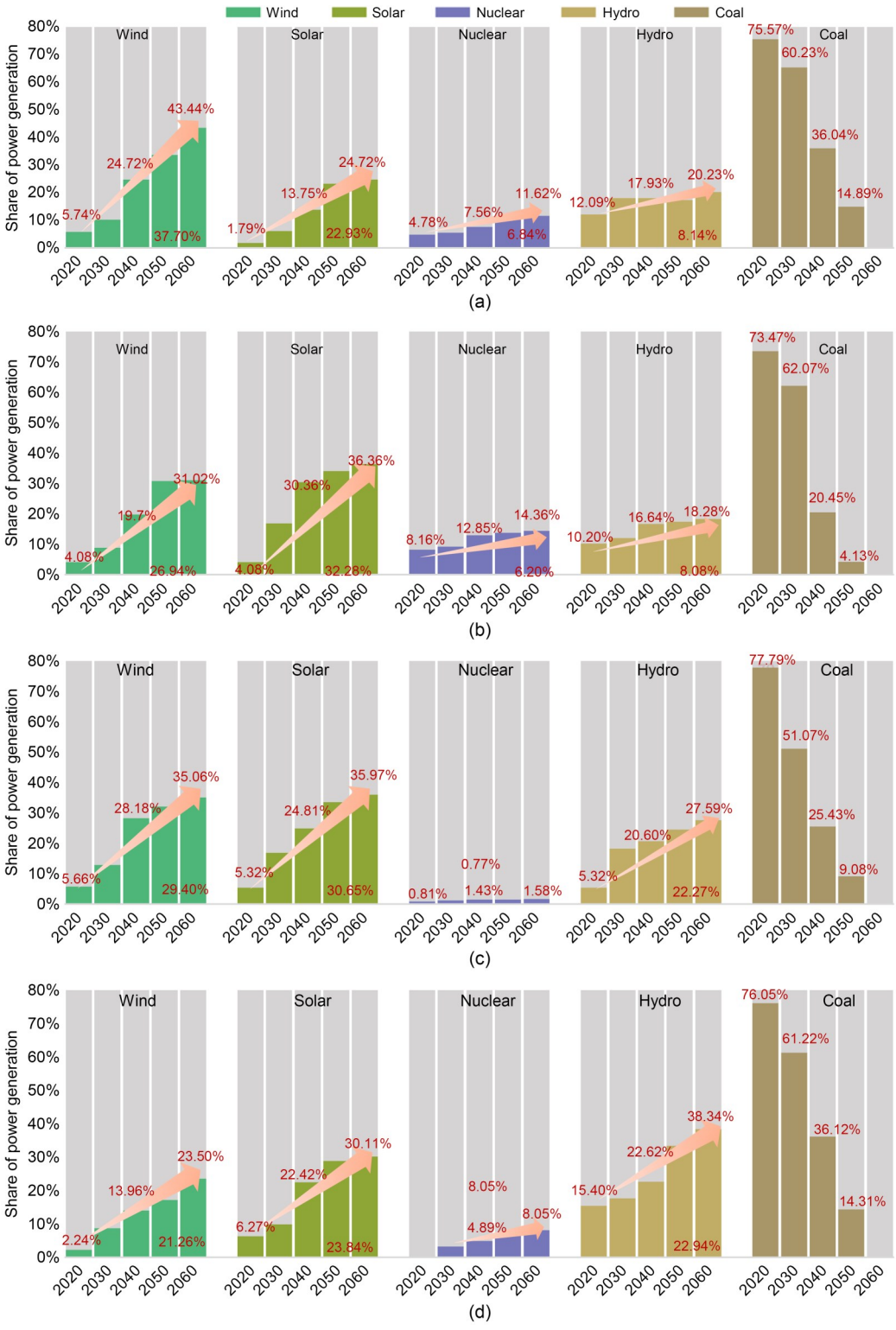

Fig. 4 Changes in the power generation structure of the four regions from 2020 to 2060 in the (a) LH region, (b) HH region, (c) LL region, and (d) HL region

Fig. 5 displays the marginal costs and cost growth rates of carbon reduction in the four regions under different peak years. The bar graph illustrates the growth rate of the cost per unit of carbon reduction, revealing

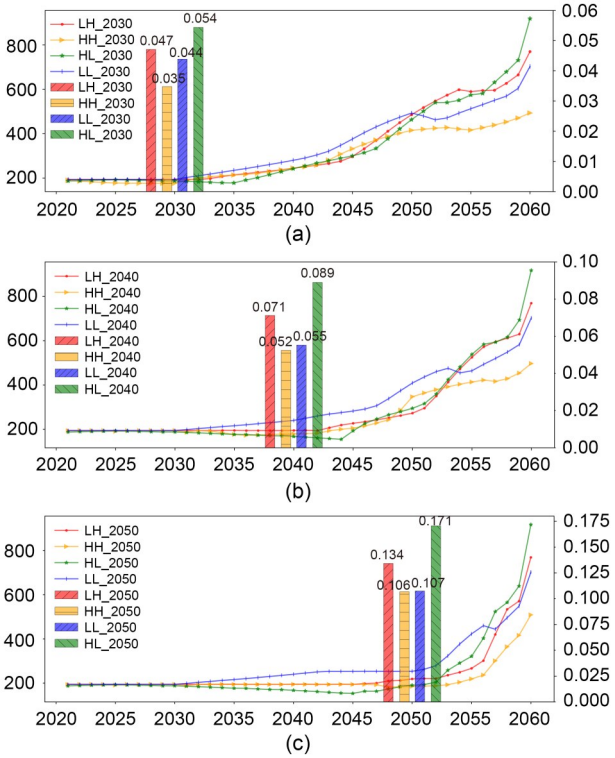

Fig. 5 Marginal cost and cost growth rate of carbon reduction under different peak years of (a) 2030, (b) 2040, and (c) 2050; (c) Marginal cost of carbon emission in peak of 2050. The left longitudinal axis represents the marginal cost of carbon emission for each year, and the right longitudinal axis represents cost growth rates of carbon reduction (unit: CNY/t)

that the growth rate increases with the delay of the peak year across all types of regions. This may be attributed to the necessity for more expensive technologies and targeted policy measures to achieve large-scale reductions in emissions within a compressed timeline. The curve delineates the annual marginal cost of carbon reduction, indicating that the marginal costs for the four distinct regions descend in the following order in 2060: HL, LH, LL, and HH. This order is consistent with the cost growth rate values across the same peak years for each region. The HL region exhibits the highest marginal costs and cost growth rates, which likely stem from Shaanxi's overdependence on thermal power and delayed deployment of alternative energy sources. This results in insufficient early-stage technological substitution, which may cause later-stage reliance on premium decarbonization solutions such as carbon capture. Conversely, it should be noted that the HH region may have achieved path optimization through a high proportion of clean energy penetration and later relied more on grid flexibility than novel emission reduction technologies.

Furthermore, Fig. 6 illustrates the total cost per unit of carbon reduction across different peak years. By 2060, the cumulative total cost increases with the deferral of the peak year. Additionally, this trend may obscure certain implicit costs: for instance, delayed peaking leads to an accumulation of carbon emissions between 2030 and 2050, potentially exacerbating the frequency of extreme climate events and elevating ecological restoration expenditures. Regardless of the peak year, the cumulative cost per unit of carbon reduction by 2060 for the four regions ranks from the highest to lowest as follows: LL, LH, HL, and HH. The LL region exhibits the highest costs due to its dual structural constraints: core cities (e.g., Beijing, Shanghai, and Chongqing) face spatial limitations and elevated costs for cross-regional green power allocation, perpetuating their partial reliance on high-carbon energy inputs, while peripheral provinces (e.g., Gansu Province, Qinghai Province, and Ningxia Hui Autonomous Region) suffer from inadequate fiscal investment and outdated power grid infrastructure, resulting in an insufficient renewable energy development rate. This bifurcated system sustains elevated decarbonization expenditures across the LL region.

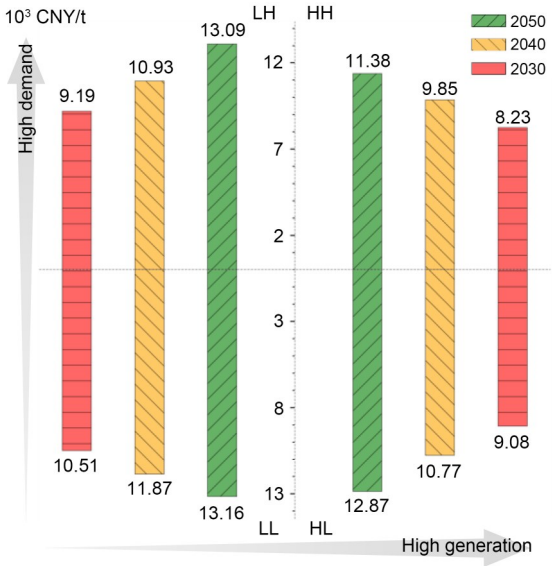

Fig. 6 Cumulative cost per unit of carbon reduction under different peak years (the first quadrant represents the LH region, the second quadrant represents the HH region, the third quadrant represents the LL region, and the fourth quadrant represents the HL region)

3.4 Energy intensity and cost change sensitivity analysis

Here, a sensitivity analysis is conducted on the rate of reduction in energy intensity and the changes in generation costs across different regions. In Fig. 7, the horizontal axis represents time in years, and the vertical axis represents the rate of reduction in energy intensity. The numbers within the heatmap indicate the cost sensitivity values corresponding to specific years and rates of energy intensity reduction.

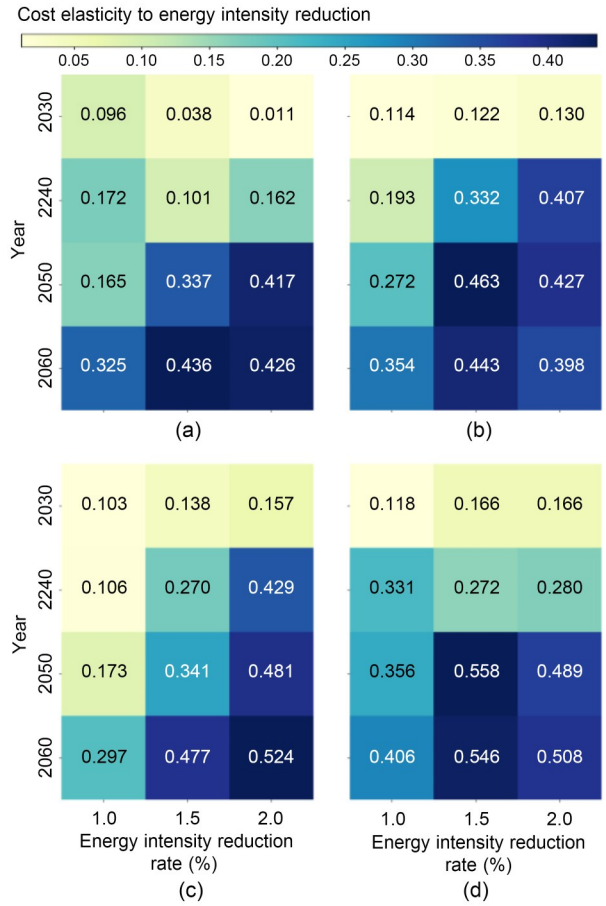

Fig. 7 Sensitivity heatmap of energy intensity and cost changes from 2020 to 2060 in the (a) LH region, (b) HH region, (c) LL region, and (d) HL region

Our analysis reveals a trend of increasing sensitivity across all regions over time, indicating that the financial impacts of reducing energy intensity are expected to grow significantly by 2060. Regional analysis reveals that the LH, HH, and HL regions exhibit maximal sensitivity at a 1.5% rate of reduction in energy intensity, suggesting optimal economic outcomes at this rate. The LL region reaches its economic optimum when the energy intensity reduction rate escalates to 2%. It is therefore recommended that the LL region set a reduction target that exceeds the national average energy intensity reduction rate. Furthermore, assuming an optimal rate of energy intensity reduction, high energy generation regions are expected to realize their maximum benefits by 2050. Thus, these regions might consider accelerating their efforts to reduce energy intensity. On the other hand, regions with low energy generation are advised to maintain their current reduction pace until 2060 to obtain the maximum economic advantage.

4 Conclusions

This study evaluated the future impact of carbon emission reduction efforts in China across supply and demand within regions with different electricity characteristics under carbon neutrality goals and provided targeted policy recommendations. We categorized provinces into four distinct regions by their electricity characteristics and formulated scenarios including BAU, DSM, GSO, NZE, and BSO. We assessed future shifts in industries' electricity consumption, adaptations in power generation mixes, the marginal cost of carbon reduction across varying peak years, and the interplay between energy intensity and cost dynamics. Our analysis integrated natural resource constraints, providing a more realistic assessment of future development. We evaluated how varying peak year timings affect carbon reduction costs and determined optimal energy intensity reduction rates for the different regions.

From an industrial development standpoint, industries within the LH region may encounter transformative pressures or declines, necessitating the strategic development of emerging economic drivers and industrial restructuring to prevent deindustrialization. Conversely, industrialization efforts in the remaining three regions are ongoing, emphasizing the need to integrate technological innovations to promote clean industrial growth. Moreover, urbanization is expected to steadily increase residential electricity demand across all regions, so a sustainable electricity supply will be required to meet this demand.

Renewable energy development plays a pivotal role in the structural transformation of China's electricity sector, as the accelerated adoption of wind and solar energy aligns with international objectives for

sustainable development and the transition to clean energy. Considering the differences in resource conditions across regions, energy strategies should be tailored to local circumstances. In resource-constrained areas, priority should be given to nuclear power and other established energy generation methods to address electricity supply shortages.

Postponing the peak year of carbon emissions increases the short-term marginal cost of carbon reduction and cumulative unit costs. Moreover, achieving a carbon peak as early as possible is economically and technologically prudent for avoiding compounding costs from climate extremes and ecological restoration work. The regional heterogeneity in marginal costs and cost growth rates across power system typologies requires tailored strategies. Specifically, the HL region, which exhibits both high marginal costs and rapid cost escalation, requires enhanced national policy support and prioritized investment.

The impact of energy intensity reduction rates varies across regions, necessitating strategic adjustments that are fitted to regional disparities. Specifically, the LH, HH, and HL regions should focus on achieving cost optimization with an energy intensity reduction rate of 1.5%, while the LL region would likely benefit from a 2.0% reduction rate. Additionally, regions with high energy generation should aim to sustain their energy intensity reduction rate beyond 2050, requiring proactive development and implementation of adaptable strategies. In contrast, low energy generation regions will need continued policy support to maintain their reduction rates.

Although this study provides an in-depth analysis of optimization pathways and strategies for supply- and demand-side emission reductions, a few limitations still exist. First, while our assumptions are based on relevant policy documents, the long-term forecast may be somewhat conservative, as it does not fully account for potential technological breakthroughs and rapid policy adjustments. Second, our study primarily involved macro-level analysis and did not fully consider regional differences or fine temporal resolution. There are significant variations in electricity demand, resource endowment, and economic development across different regions. Thus, a goal for future research is to optimize the results at a more granular level, particularly by incorporating regional differentiation factors and higher-resolution models. Moreover, expanding the scope to include sectoral interactions and assessing the implications of emerging technologies (such as energy storage, carbon capture, and smart grid innovations) would offer a more comprehensive understanding of the power system's shift towards carbon neutrality.

Acknowledgments

This work is supported by the Fundamental Research Funds for the Central Universities (No. 226-2024-00017), the National Natural Science Foundation of China (No. 52206281), and the Zhejiang Provincial Natural Science Foundation of China (No. LY24E060002). Numerical computations were performed at the Hefei Advanced Computing Center, China.

Author contributions

Xuanxuan MING designed the research, processed the corresponding data, and wrote the first draft of the manuscript. Qiang WANG and Kun LUO helped to organize the manuscript. Xuanxuan MING and Xinhao DU revised and edited the final version. Jianren FAN supervised the manuscript.

Conflict of interest

Jianren FAN is an Editorial Board member of this journal, and is NOT involved in the editorial review or the decision to publish this article. Xuanxuan MING, Qiang WANG, Kun LUO, Xinhao DU, and Jianren FAN declare that they have no conflict of interest.

References

Awopone AK, Zobaa AF, Banuenumah W, 2017. Assessment of optimal pathways for power generation system in Ghana. *Cogent Engineering*, 4(1):1314065. https://doi.org/10.1080/23311916.2017.1314065

Besagni G, Borgarello M, Premoli Vilà L, et al., 2020. Moirae–bottom-up model to compute the energy consumption of the italian residential sector: model design, validation and evaluation of electrification pathways. *Energy*, 211:118674. https://doi.org/10.1016/j.energy.2020.118674

Cai LY, Duan JL, Lu XJ, et al., 2022. Pathways for electric power industry to achieve carbon emissions peak and carbon neutrality based on LEAP model: a case study of state-owned power generation enterprise in China. *Computers & Industrial Engineering*, 170:108334. https://doi.org/10.1016/j.cie.2022.108334

China Electricity Council, 2021. China Electric Power Yearbook 2020. China Electric Power Press, Beijing, China (in Chinese).

Elsisi M, Abdelfattah H, 2020. New design of variable structure control based on lightning search algorithm for nuclear reactor power system considering load-following operation. *Nuclear Engineering and Technology*, 52(3): 544-551. https://doi.org/10.1016/j.net.2019.08.003

Fan JL, Li Z, Huang X, et al., 2023. A net-zero emissions strategy for China's power sector using carbon-capture utilization and storage. *Nature Communications*, 14(1): 5972.

https://doi.org/10.1038/s41467-023-41548-4

Goldemberg J, Prado LTS, 2013. The decline of sectorial components of the world's energy intensity. *Energy Policy*, 54:62-65. https://doi.org/10.1016/j.enpol.2012.11.023

Handayani K, Anugrah P, Goembira F, et al., 2022. Moving beyond the NDCs: ASEAN pathways to a net-zero emissions power sector in 2050. *Applied Energy*, 311:118580. https://doi.org/10.1016/j.apenergy.2022.118580

Handayani K, Overland I, Suryadi B, et al., 2023. Integrating 100% renewable energy into electricity systems: a net-zero analysis for Cambodia, Laos, and Myanmar. *Energy Reports*, 10:4849-4869. https://doi.org/10.1016/j.egyr.2023.11.005

IPCC (The Intergovernmental Panel on Climate Change), 2023. Ar6 Synthesis Report: Climate Change 2023. IPCC, Geneva, Switzerland.

Jia XP, Zhang YM, Tan RR, et al., 2022. Multi-objective energy planning for China's dual carbon goals. *Sustainable Production and Consumption*, 34:552-564. https://doi.org/10.1016/j.spc.2022.10.009

Lee EK, Mitchell JE, 2009. Integer programming: branch and bound methods. *In*: Floudas CA, Pardalos PM (Eds.), Encyclopedia of Optimization. Springer, New York, USA, p.1634-1643. https://doi.org/10.1007/978-0-387-74759-0_286

Li LH, Zhang Y, Zhou TJ, et al., 2022. Mitigation of China's carbon neutrality to global warming. *Nature Communications*, 13(1):5315. https://doi.org/10.1038/s41467-022-33047-9

Liu LB, Wang Y, Wang Z, et al., 2022. Potential contributions of wind and solar power to China's carbon neutrality. *Resources, Conservation and Recycling*, 180:106155. https://doi.org/10.1016/j.resconrec.2022.106155

Ma YM, Wang HX, Hong F, et al., 2021. Modeling and optimization of combined heat and power with power-to-gas and carbon capture system in integrated energy system. *Energy*, 236:121392. https://doi.org/10.1016/j.energy.2021.121392

Ming XX, Wang Q, Luo K, et al., 2024. An integrated economic, energy, and environmental analysis to optimize evaluation of carbon reduction strategies at the regional level: a case study in Zhejiang, China. *Journal of Environmental Management*, 351:119742. https://doi.org/10.1016/j.jenvman.2023.119742

National Bureau of Statistics of China, 2020. Statistical Yearbook of China 2021. China Statistics Press, Beijing, China (in Chinese).

National Bureau of Statistics of China, 2021. China Population Census Yearbook 2020. China Statistics Press, Beijing, China (in Chinese).

Rao YC, Wang XL, Li HK, 2024. Forecasting electricity consumption in China's Pearl River Delta urban agglomeration under the optimal economic growth path with low-carbon goals: based on data of NPP-VIIRS-like nighttime light. *Energy*, 294:130970. https://doi.org/10.1016/j.energy.2024.130970

Rogan F, Cahill CJ, Daly HE, et al., 2014. Leaps and bounds—an energy demand and constraint optimised model of the Irish energy system. *Energy Efficiency*, 7(3):441-466. https://doi.org/10.1007/s12053-013-9231-9

Saltelli A, 2002. Sensitivity analysis for importance assessment. *Risk Analysis*, 22(3):579-590. https://doi.org/10.1111/0272-4332.00040

Saltelli A, Ratto M, Andres T, et al., 2007. Global Sensitivity Analysis: the Primer. John Wiley, Chichester, UK.

Schäfer AW, Evans AD, Reynolds TG, et al., 2016. Costs of mitigating CO_2 emissions from passenger aircraft. *Nature Climate Change*, 6(4):412-417. https://doi.org/10.1038/nclimate2865

Wang GZ, 2018. Population Projection Methods and Applications. Social Sciences Academic Press, Beijing, China (in Chinese).

Wang Q, Luo K, Yuan RY, et al., 2020. A multiscale numerical framework coupled with control strategies for simulating a wind farm in complex terrain. *Energy*, 203:117913. https://doi.org/10.1016/j.energy.2020.117913

Wang Q, Luo K, Wu CL, et al., 2023. Inter-farm cluster interaction of the operational and planned offshore wind power base. *Journal of Cleaner Production*, 396:136529. https://doi.org/10.1016/j.jclepro.2023.136529

Wang XG, Lu ZM, Li TX, et al., 2023. Carbon-neutral power system transition pathways for coal-dominant and renewable resource-abundant regions: Inner Mongolia as a case study. *Energy Conversion and Management*, 285:117013. https://doi.org/10.1016/j.enconman.2023.117013

Wu W, Zhang TT, Xie XM, et al., 2021. Regional low carbon development pathways for the Yangtze River Delta region in China. *Energy Policy*, 151:112172. https://doi.org/10.1016/j.enpol.2021.112172

Yang Y, Zhang C, Qiu J, 2023. Low-carbon system transition considering collaborative emission reduction on supply-demand side. IEEE International Conference on Energy Technologies for Future Grids (ETFG), p.1-6. https://doi.org/10.1109/ETFG55873.2023.10408546

Yap KY, Sarimuthu CR, Lim JMY, 2020. Artificial intelligence based MPPT techniques for solar power system: a review. *Journal of Modern Power Systems and Clean Energy*, 8(6):1043-1059. https://doi.org/10.35833/MPCE.2020.000159

Yu XY, Dong ZJ, Zhou DQ, et al., 2021. Integration of tradable green certificates trading and carbon emissions trading: how will Chinese power industry do? *Journal of Cleaner Production*, 279:123485. https://doi.org/10.1016/j.jclepro.2020.123485

Zhou JH, He YX, Lyu Y, et al., 2023. Long-term electricity forecasting for the industrial sector in western China under the carbon peaking and carbon neutral targets. *Energy for Sustainable Development*, 73:174-187. https://doi.org/10.1016/j.esd.2023.02.003

Zhou WD, Zhuang GY, Liu LB, 2023. Comprehensive assessment of energy supply-side and demand-side coordination on pathways to carbon neutrality of the Yangtze River Delta in China. *Journal of Cleaner Production*, 404:136904. https://doi.org/10.1016/j.jclepro.2023.136904

Electronic supplementary materials

Table S1, Fig. S1